International Journal of Mechanical Sciences 255 (2023) 108461

Contents lists available at ScienceDirect

International Journal of Mechanical Sciences

journal homepage: www.elsevier.com/locate/ijmecsci

# On the contact between elasto-plastic media with self-affine fractal roughness

G. Violano [a,b,*], L. Afferrante [a]

[a] Department of Mechanics, Mathematics and Management, Polytechnic University of Bari, Via E. Orabona, 4, 70125, Bari, Italy

[b] Department of Materials Science and Engineering, Saarland University, 66123, Saarbrücken, Germany

ARTICLE INFO

*Keywords:*
Plasticity
Surface roughness
Contact mechanics
Asperity

ABSTRACT

Modeling the elasto-plastic contact between rough interfaces may require high computational effort as real surfaces present broad roughness spectra. In this work, we propose an efficient multi-asperity model where each asperity follows Jackson and Green's equations and both coupling and coalescence of contact spots are considered. In agreement with previous studies, the contact area $A$ is found to rise linearly with the applied load. Moreover, under the assumption of yield stress independent of the asperity size, no differences are found with respect to the elastic contact solution for nanometric root mean square (rms) roughness amplitudes $h_{\text{rms}}$. On the contrary, for micrometric $h_{\text{rms}}$, the slope of the area-load relation is observed to increase when reducing the yield strength $\sigma_{\text{Y}}$. We have also investigated the effect of increasing the rms roughness gradient of the surface $h'_{\text{rms}}$ by adding fine-scale wavelengths to the roughness spectrum. Due to plastic deformations, the contact area $A$ is found to be independent of the high-frequency cut-off of the roughness spectrum as it converges when increasing the number of roughness scales.

## 1. Introduction

Contact mechanics between nominally flat surfaces of elastic media is now well understood [1–4]. Existing theories and models have shown that, under frictionless conditions, the real contact area $A$ increases linearly with the normal applied load $F$ according to $A \sim 2F/(E^* h'_{\text{rms}})$, being $E^*$ the composite elastic modulus of contacting materials and $h'_{\text{rms}}$ the root mean square (rms) gradient of the surface roughness. Deviation from linearity are observed when $A/A_0 > 0.2 - 0.3$, being $A_0$ the nominal contact area [4].

The rms gradient increases by adding shorter and shorter wavelengths to roughness spectrum, whose truncation frequency defines the total number $N$ of roughness scales. For purely elastic media, theoretical models predict zero contact area in the fractal limit [5,6], namely when $N \to \infty$. However, for real surfaces, fractal limit will not be reached for two main reasons. First, atomic scale represents the natural truncation of roughness spectrum. Second, at higher loads, we expect that plasticity destroys shorter wavelengths.

Plasticity plays a key role in a tremendous number of applications and at different length scales. Understanding nanoscale plasticity is of crucial importance for developing miniaturized smarter technologies [7]. At the microscale, plasticity may affect the reliability of micro electro-mechanical systems [8]. At larger scales, plastic deformations at the asperity level are observed when surfaces are subjected to high contact pressure as, for example, occur in metallic seals [9].

Natural and manufactured surfaces present roughness spectra that may extend on several length scales [10]. As a result, modeling realistic rough interfaces require fine discretization, which in turns leads to high computational demand [11].

Over the last years, several methods have been proposed to solve elasto-plastic contacts between rough surfaces. Among the first approaches, statistical and microcontact models [12–14] overcome computational issues, but suffer from strong assumptions, such as simplistic description of surface roughness and absence of coupling between surface asperities. In fact, these models are based on a bearing area approach, which is only valid in limiting cases but not applicable to generic, randomly rough surfaces [4].

Overcoming the limits of bearing area models, Persson [15] developed a multiscale theory where broad roughness spectra can be considered and plastic deformation occurs if the mean applied stress exceeds the yield strength $\sigma_{\text{Y}}$ of the material, which is assumed to exhibit an elastic-perfectly plastic constitutive behavior. Recently, Xu et al. [16] proposed closed-form solutions of Persson's elasto-plastic theory, which is solved by a superposition of three Gaussian functions.

Carvalho et al. [17] proposed a multiscale algorithm based on the split of the roughness spectrum; the algorithm can estimate the real contact area from a given database of contact area fraction and pressure values. The authors applied their model to study the elasto-plastic response of a material with a $J_2$ isotropic plasticity law.

* Corresponding author at: Department of Mechanics, Mathematics and Management, Polytechnic University of Bari, Via E. Orabona, 4, 70125, Bari, Italy.
*E-mail address:* guido.violano@poliba.it (G. Violano).

https://doi.org/10.1016/j.ijmecsci.2023.108461
Received 19 January 2023; Received in revised form 10 May 2023; Accepted 10 May 2023
Available online 13 May 2023
0020-7403/

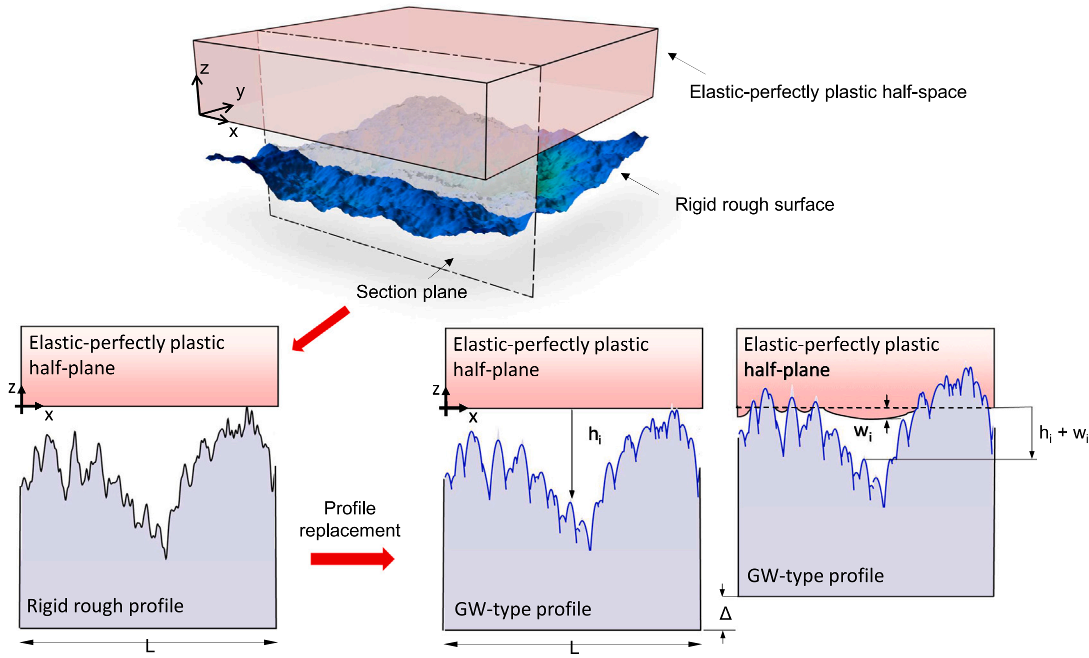


**Fig. 1.** A sketch of the problem under investigation: a rigid rough surface is pressed into an elastic-perfectly plastic half-space. The initial surface is replaced by a set of paraboloids of revolution whose position and height are coincident with those of the asperities summits. The origin of the coordinate system $Oxyz$ is placed at the highest peak of the surface with the $z$-axis oriented upwards. Therefore, the initial distance $h_i$ between the asperities and the flat half-space is negative, and the rigid approach $\Delta$ and displacement $w_i$ are taken positive when agreeing with the orientation of the $z$-axis.

With their pioneering finite element (FE) approach, Pei et al. [18] studied the normal contact between a rigid plane and an elasto-plastic solid with self-affine fractal surface. They found that the contact area $A$ rises linearly with the applied load.

More recently, Zhang et al. [19] developed FE models to simulate the contact between aluminum and polycarbonate interfaces, finding a good agreement with X-ray tomography measurements of the contact area.

Liang et al. [20] proposed an incremental equivalent contact model for elastic-perfectly plastic solids with rough surfaces, comparing theoretical predictions with FE calculations of the contact area. They also observed linearity of the area-load relation in their calculations.

Despite their accuracy, FE simulations are extremely time consuming (see, for example, the discussion in Ref. [11]). To overcome this issue, Frérot et al. [21] recently developed a Fourier-accelerated volume integral method, which allows to handle fine discretization and reduce computation time costs.

Zhang et al. [22] developed a hybrid FE-multiasperity approach to solve rough elasto-plastic contacts, considering the deformation behavior affected by the asperities size. A similar strategy has been adopted in Ref. [23].

In Ref. [24], a boundary element (BE) method was proposed to study the elasto-plastic contact between 1D rough profiles. A similar problem has been addressed in Refs. [25,26], where Green's function molecular dynamics is combined with discrete-dislocation plasticity to capture size-dependent plasticity. More recently, Tiwari et al. [27] exploited a BE method to model the contact between 2D rough surfaces, studying how roughness is modified by the plastic flow.

In this work, we extend Interacting and Coalescing Hertzian Asperities (ICHA) model [28] to take into account plastic deformations occurring at the asperity level. Such problem is of practical interest for metallic interfaces presenting micro(nano)metric roughness [27, 29]. ICHA model showed high accuracy in predicting elastic contact mechanics between randomly rough 2D surfaces [4]. The model conveniently implements elastic coupling between asperities and coalescing of contact spots and is extremely efficient, running very fast on common PC [4].

Recently, Zhang et al. [30] performed FE simulations of two adjacent elasto-plastic asperities squeezed by a rigid flat. They showed that coalescence strongly affects contact stiffness. Even assuming a linear-elastic behavior, coalescence is fundamental to capture contact mechanical response of realistic surfaces with roughness extending on several wavelengths [4,31,32].

The original version of ICHA model does not include plastic deformations. Over the last years, different models have been proposed to describe the elasto-plastic contact mechanics of a single asperity [33–35], and we refer the reader to recent comprehensive reviews [36,37]. Here, we extend ICHA model assuming that each asperity behaves according to the well established Jackson & Green model (JG) [35]. Such choice is motivated by the fact that JG equations have been validated with experiments and consider the evolution of hardness during contact.

We, therefore, investigate the effect of plasticity in the contact of realistic fractal geometries with micro(nano)metric roughness amplitudes.

## 2. Formulation

Consider a linear elastic-perfectly plastic half-space squeezed against a rigid randomly rough surface (Fig. 1).

Roughness is described by a self-affine isotropic fractal geometry. Under such an assumption, the morphology of the surface topography remains unaffected by a scale change and it is independent of measuring direction. It is convenient to describe surface roughness by means of its power spectral density (PSD). Specifically, we assume a PSD

$$\begin{aligned} C(q) &= C_0 && \text{for} \quad q_L \le q < q_0 \\ C(q) &= C_0 \left(q/q_L\right)^{-2(H+1)} && \text{for} \quad q_0 \le q < q_1, \end{aligned} \tag{1}$$

and zero otherwise. The quantity $q$ is the modulus of the wave vector $\mathbf{q} = (q_x, q_y)$. With $q_L = 2\pi/L$ and $q_0$ we denote the moduli of the cut-off and roll-off wave vector, being $L$ the lateral size of the system (we assumed a square domain with $L_x = L_y = L$). The high-frequency cut-off is $q_1 = N q_L$, where $N$ is the number of roughness scales. Finally, $H$ is the Hurst exponent, which is related to the fractal dimension $D_f = 3 - H$.

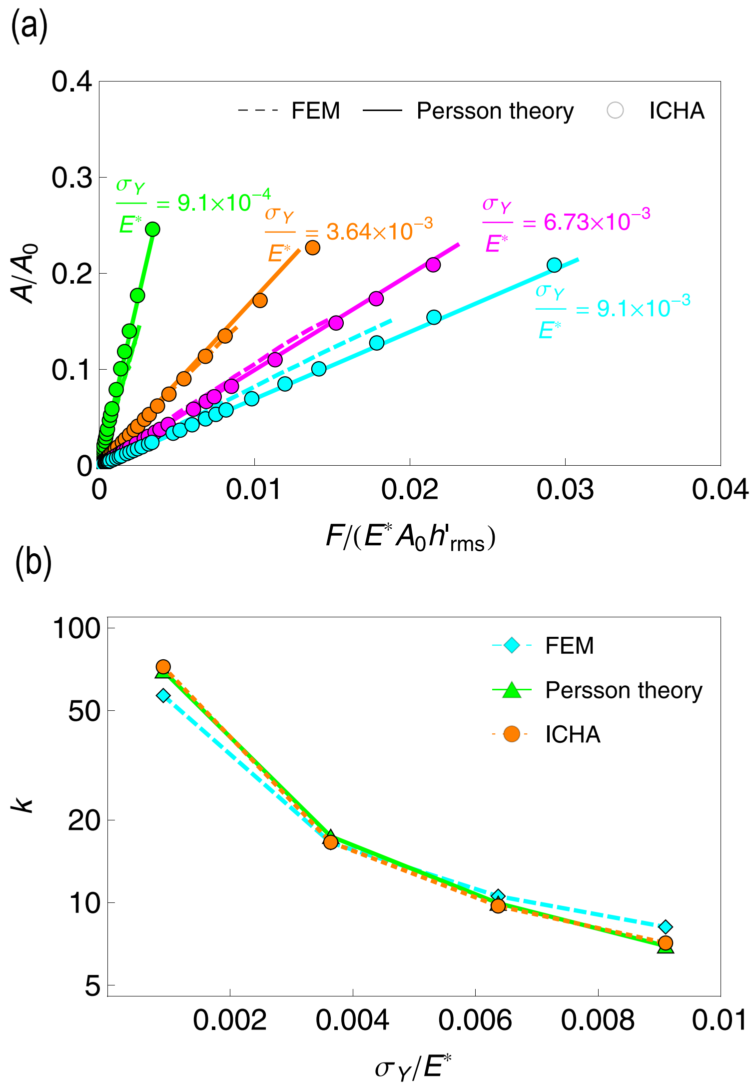


**Fig. 2.** (a) The normalized contact area $A/A_0$ as a function of the adimensional applied load $F/(E^* A_0 h'_{rms})$. Markers refer to ICHA model, while solid and dashed lines denote Persson's theory and FE model predictions, respectively. Details about the specific method and parameters of FE simulations can be found in Ref. [20]. Note the value of $h'_{rms}$ used for FE data is taken from Ref. [38]. Results are shown for pure power law fractal surfaces with $h_{rms} = 500$ nm, $H = 0.5$, $N = 128$, and $L = 200$ μm. Material properties are $E = 100$ GPa, $\nu = 0.3$ and $\sigma_Y/E^* = (0.91,\ 3.64,\ 6.73,\ 9.1) \times 10^{-3}$. (b) The slope $k$ of the area-load curves shown in (a); results are given in terms of the normalized stress $\sigma_Y/E^*$.

### 2.1. Elasto-plastic contact of a single asperity

Jackson & Green (JG) performed a comprehensive finite element (FE) study of the contact between an elastic-perfectly plastic sphere and a rigid half-space [35]. Simulations were carried out for a wide range of material properties, typical of engineering applications. On the basis of FE results, JG derived a theoretical (phenomenological) contact model, whose predictions were found to be in good agreement with numerical and experimental data.

The point of first yielding is theoretically derived according to the von Mises yield criterion and is defined by a critical penetration of the sphere in the half-space. At first yielding, the critical penetration $\delta_c$, contact area $A_c$ and applied load $F_c$ are

$$\delta_c = \left(\frac{\pi c \sigma_Y}{2E^*}\right)^2 R;\ A_c = \pi^3 \left(\frac{c\sigma_Y R}{2E^*}\right)^2;\ F_c = \frac{4}{3}\left(\frac{R}{E^*}\right)^2 \left(\frac{c}{2}\pi\sigma_Y\right)^3, \tag{2}$$

where $R$ is the radius of curvature of the sphere, $\sigma_Y$ is the yield strength of the material, and $E^* = E/(1-\nu^2)$ is the composite elastic modulus, being $E$ Young's modulus and $\nu$ Poisson's ratio of the elasto-plastic material. Finally, to capture the dependence with $\nu$, JG introduced the empirical parameter $c = 1.295\exp(0.736\nu)$. In the following, we shall adopt the same adimensional parameters of JG, i.e.,

$$\bar{\delta} = \delta/\delta_c;\ \bar{A} = A/A_c;\ \bar{F} = F/F_c \tag{3}$$

Despite $\bar{\delta}_c$ identifies the point of first yielding, JG observed that the transition from elastically dominant behavior to elasto-plastic one occurs when $\bar{\delta} = \bar{\delta}_t = 1.9$. As a result, the elastic range is assumed to hold for $0 < \bar{\delta} \le \bar{\delta}_t$, where contact is described by Hertz theory; the normalized contact area $\bar{A}$ and applied load $\bar{F}$ are, therefore, (Ref. [39])

$$\bar{A} = \bar{\delta} \tag{4}$$

$$\bar{F} = \bar{\delta}^{3/2} \tag{5}$$

For penetration $\bar{\delta} > \bar{\delta}_t$, plastic deformation are no longer negligible and the contact quantities are returned by the following relations obtained in Ref. [35] as fit of FE data

$$\bar{A} = \bar{\delta}(\bar{\delta}/\bar{\delta}_t)^B \tag{6}$$

$$\bar{F} = \{\left[\exp(-0.25(\bar{\delta})^{5/12})\right](\bar{\delta})^{3/2} +$$

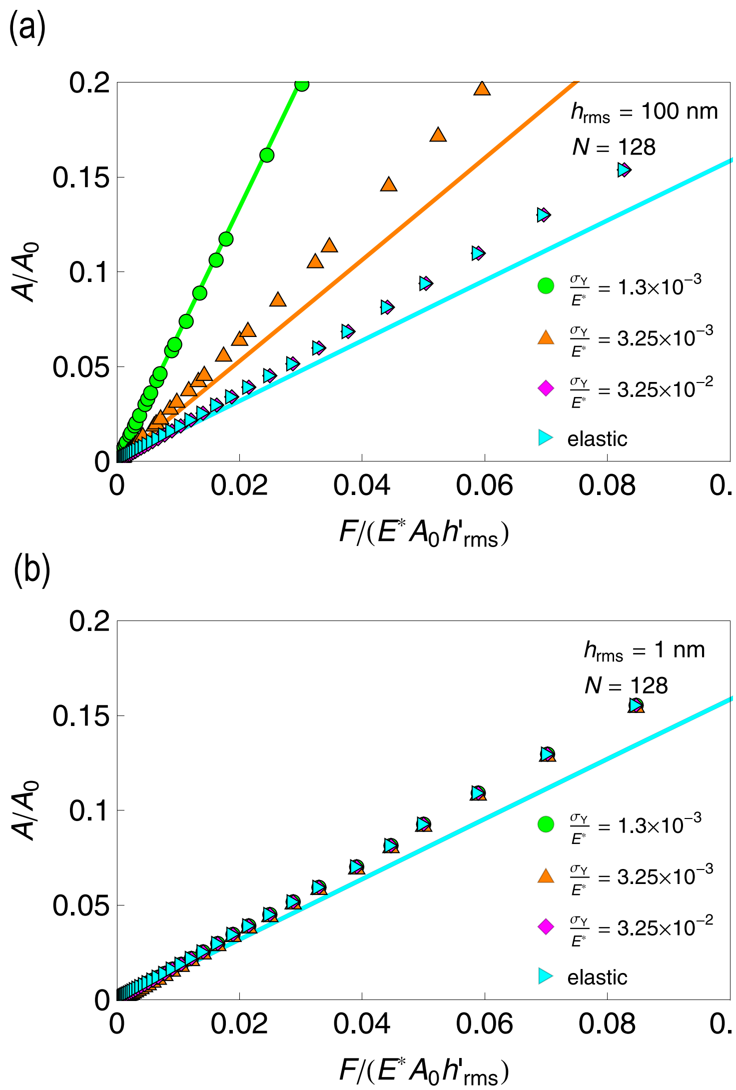


**Fig. 3.** The normalized contact area $A/A_0$ as a function of the adimensional applied load $F/(E^* A_0 h'_{\mathrm{rms}})$. Markers refer to ICHA model, while solid lines denote Persson's theory predictions. Results are shown for fractal surfaces with $H = 0.8$, $N = 128$, $L = 200$ μm, $q_0 = 2q_L$, with $h_{\mathrm{rms}} = 100$ nm (a) and $h_{\mathrm{rms}} = 1$ nm (b). Material properties are $E = 70$ GPa, $\nu = 0.3$ and $\sigma_Y/E^* = (1.3,\ 3.25,\ 32.5) \times 10^{-3}$.

$$4H_G\left[1-\exp(-0.04(\bar{\delta})^{5/9})\right](\bar{\delta})/(c\sigma_Y)\}, \tag{7}$$

where the constant $B = 0.14\exp(23e_Y)$ is a fit parameter depending on $e_Y = \sigma_Y/E^*$.

In Eq. (7), the contact hardness $H_G$, which is commonly approximated to be a material constant ($H_G \sim 2.8\ \sigma_Y$), actually varies during contact as it depends on the penetration according to the empirical law

$$H_G = 2.84\sigma_Y\left[1-\exp\left(-0.82\left(\frac{\pi c e_Y}{2}\sqrt{\bar{\delta}}\left(\frac{\bar{\delta}}{\bar{\delta}_t}\right)^{B/2}\right)\right)^{-0.7}\right]. \tag{8}$$

Note the present formulation assumes the plasticity is size-independent. As an example, this assumption can be used to describe the mechanical properties of specific metallic alloys [40–43]. However, it is known that the yield stress can be a function of the asperity size at the micrometric scales [44–47], making higher the elastic limit for smaller asperities.

### 2.2. Elasto-plastic rough contact: the ICHA multi-asperity model

According to ICHA model [28], the rough surface is replaced by a set of paraboloids of revolution whose position and height are coincident with those of the asperities summits (see schematic plot in Fig. 1). The curvature $\kappa$ of each paraboloid is computed as the geometric mean of the principal curvatures of the corresponding asperity, that is we calculate $\kappa$ as the root square of the first order approximation of the Gauss curvature: $\kappa = \sqrt{(k_x k_y - k_{xy})}$, where $k_x$, $k_y$ and $k_{xy}$ are the curvature in the $x$ and $y$ direction and the 'composite' curvature, respectively. Note the curvatures will depend on the surface discretization as they are computed from the heights on the initial mesh grid by eqs. (2–4) of Ref. [28].

In the initial configuration, rigid surface's location is adjusted by imposing zero gap between the half-space surface and the highest asperity. Contact is solved under displacement controlled conditions, by increasing the approach $\Delta$ of the rigid surface in the half-space.

An asperity $i$ gets into contact if its penetration $\delta_i > 0$, being

$$\delta_i = h_i + \Delta - w_i. \tag{9}$$

In Eq. (9), $h_i$ is the asperity's height in the initial configuration and $w_i$ is the displacement due to all contacting asperities.

At the first contact, the generic contact radius is estimated by

$$a_i = \sqrt{\bar{A}_i A_{ci}/\pi}, \tag{10}$$

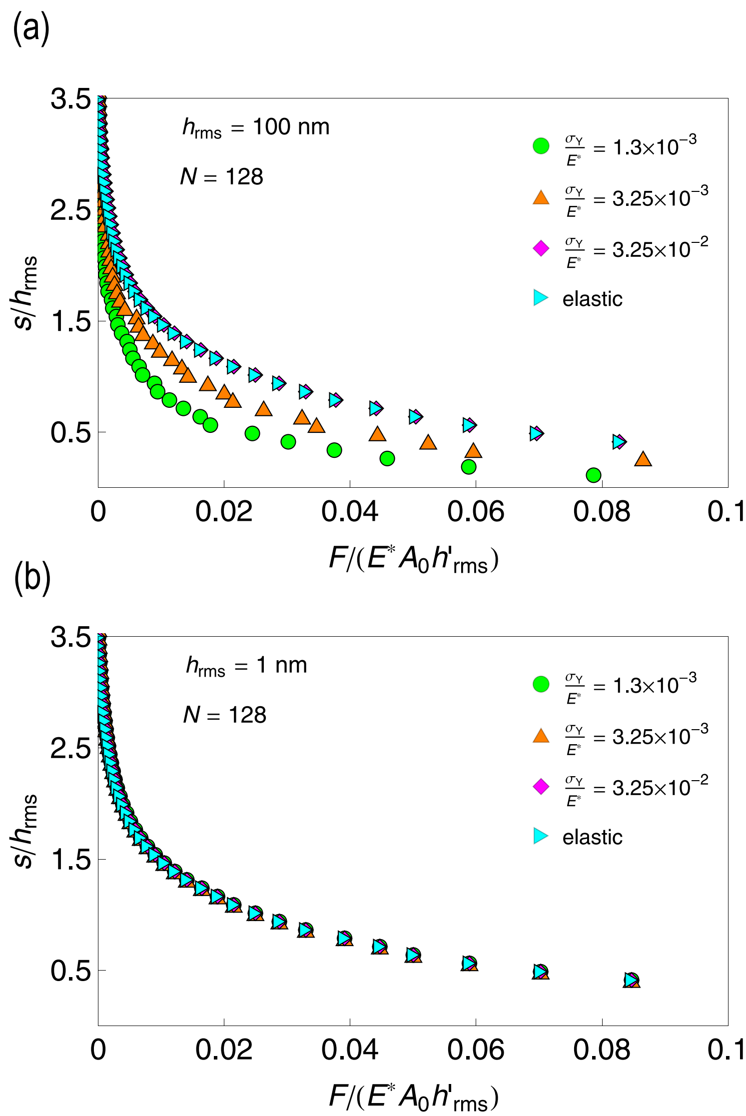


**Fig. 4.** The normalized mean separation $s/h_{\rm rms}$ as a function of the adimensional applied load $F/(E^* A_0 h'_{\rm rms})$. Results are shown for fractal surfaces with $H = 0.8$, $N = 128$, $L = 200$ μm, $q_0 = 2q_{\rm L}$, with $h_{\rm rms} = 100$ nm (a) and $h_{\rm rms} = 1$ nm (b). Material properties are $E = 70$ GPa, $\nu = 0.3$ and $\sigma_{\rm Y}/E^* = (1.3,\ 3.25,\ 32.5) \times 10^{-3}$.

where the normalized contact area $\bar{A}_i(\bar{\delta}_i)$ is returned by Eqs. (4) or (6), depending on whether we are in the elastic regime ($0 < \delta_i \leq \delta_{ti}$) or elasto-plastic one ($\delta > \delta_{ti}$). For a penetration increase $\Delta\delta_i$, the corresponding contact radius increase is calculated by exploiting the differentiation rule $\Delta a_i = \Delta\delta_i/(d\delta/da)$ [28]. The derivative $d\delta/da$ is obtained from Hertz or JG theory, after performing some basic maths on Eqs. (4)–(6). The load due to the asperity $i$ is

$$F_i = \bar{F}_i F_{ci}, \tag{11}$$

where the normalized load $\bar{F}_i(\bar{\delta}_i)$ is returned by Eq. (5), if $0 < \delta_i \leq \delta_{ti}$, and Eq. (7), if $\delta > \delta_{ti}$.

In the original formulation of ICHA model [28], $w_i$ is the sum of the local Hertzian displacement plus the contribution of all the other asperities in contact. Such procedure is based on the validity of the superposition principle, which requires the material behavior to be linear elastic.

For several engineering problems, full-contact condition is rarely reached, and real contact area is split into contact spots. In such case, we expect that plasticity is confined at the asperity level [29], while it is reasonable to assume that the gross of the half-space response is elastic [48]. As a result, we can assume that the global coupling is still elastic. A similar approach has been previously proposed by Zhao & Chang [48], where a zero$^{\rm th}$ order asperities interaction was considered. Therefore, we compute the displacement $w_i$ as the sum of the asperity local displacement $w_{i0}$ and the contribution of the other asperities in contact $w_{ij}$, so that

$$w_i = w_{i0} + w_{ij}. \tag{12}$$

In Eq. (12), the term $w_{i0}$ is

$$w_{i0} = a_i^2/R_i \tag{13}$$

in the elastic regime (Ref. [39]), and

$$w_{i0} = \delta_{ci}\left(1.9^B \pi a_i^2/A_{ci}\right)^{1/(B+1)} \tag{14}$$

in the elasto-plastic regime (from JG model [35]).

The term $w_{ij}$ can be estimated by exploiting the Boussinesq formula for concentrated load [39]; as a result

$$w_{ij} = \frac{1}{\pi E^*}\sum_{j=1, j\neq i}^{n_{\rm ac}} \frac{F_j}{r_{ij}} \tag{15}$$

where $n_{\rm ac}$ is the total number of asperities in contact and $r_{ij}$ is the distance between the asperities $i$ and $j$. Finally, the load $F_j$ due to the

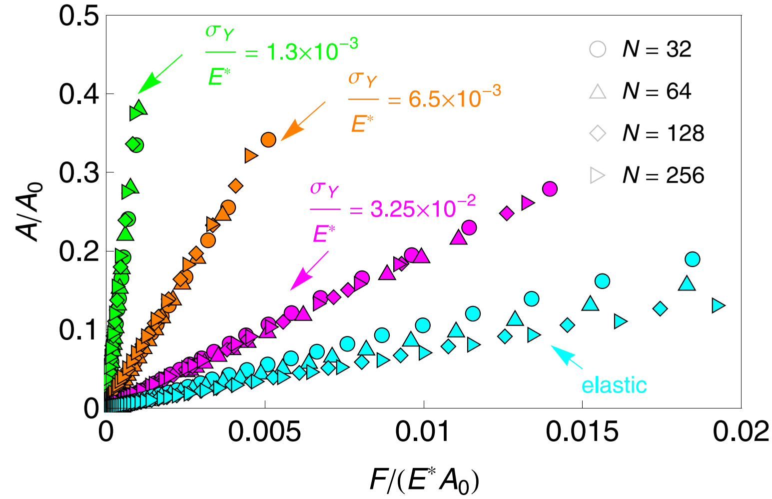


**Fig. 5.** The normalized contact area $A/A_0$ as a function of the adimensional applied load $F/(E^* A_0)$. Results are shown for fractal surfaces with $H = 0.8$, $N = 32, 64, 128, 256$, $L = 200$ μm, $q_0 = 2q_L$, and $h_{rms} = 1.04$ μm. Material properties are $E = 70$ GPa, $\nu = 0.3$ and $\sigma_Y/E^* = (1.3,\ 6.5,\ 32.5) \times 10^{-3}$.

generic asperity $j$ is given by Eq. (11). Eq. (15) is strictly valid in the elastic regime.

When an asperity undergoes plastic deformations, the term $w_{ij}$ is instead computed as the mean displacement that the load $F_j$ determines on the square domain, by exploiting Love solution (see Ref. [39]).

To capture coalescence of merging contact patches the procedure developed in ICHA model is adopted. Therefore, when two spots with contact radius $a_i$ and $a_j$ overlap, the corresponding asperities are suppressed and replaced by an equivalent macro-asperity, which maintains the same contact area ($a_{eq}^2 = a_i^2 + a_j^2$) and geometrical volume centroid. The equivalent radius of curvature is calculated with the geometrical mean $R_{eq}^2 = R_i^2 + R_j^2$. Finally, the height of the equivalent asperity is adjusted to effectively return the area $\pi a_{eq}^2$ at the given separation.

The total contact area $A$ and applied load $F$ are calculated by summing up the contribution of each asperity

$$A = \pi \sum_{i=1}^{n_c} a_i^2;\ F = \sum_{i=1}^{n_c} F_i. \tag{16}$$

In the model, a self-balanced load distribution is applied to the system to zero the mean interfacial displacement of the half-space. As a result, the mean separation $s$ is obtained by subtracting the approach of the rigid rough surface to the initial separation $s_0$, being $s = s_0 - \Delta$.

## 3. Results

First, we compare the results of the present model with those of other approaches available in the literature. Specifically, Fig. 2a shows the adimensional contact area $A/A_0$ in terms of the normalized load $F/(E^* A_0 h'_{rms})$. Dashed lines refer to the finite element (FE) predictions taken from Ref. [20], while markers denote ICHA results. Moreover, theoretical predictions of Persson's theory for elastoplastic contacts, as recently revised by Xu et al. [16], are also shown with solid lines. Results are presented for pure power law fractal surfaces (without roll-off) with $h_{rms} = 500$ nm, $H = 0.5$, $N = 128$ and $L = 200$ μm. Moreover, the elastic modulus and Poisson's ratio of the material are $E = 100$ GPa and $\nu = 0.3$, respectively.

Notice FE simulations are performed on a single realization of the surface with 200 × 200 discretization points. We have numerically generated surfaces with the same roughness parameters. However, thanks to its efficiency, ICHA data are averaged on four different realizations of the surface with 1024 × 1024 discretization points (resulting in $h'_{rms} \sim 0.147$). Even if computations have not been carried out on the same surface realization, a good agreement is observed between ICHA predictions and FE data. Interestingly, a good match is also obtained with Persson's theory, where calculations have been performed assuming a constant contact hardness $H_G = 2.8\ \sigma_Y$.

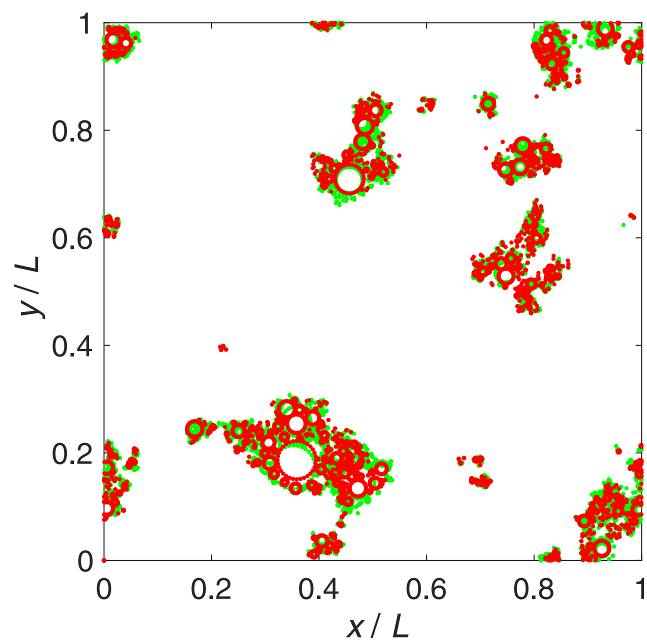


**Fig. 6.** The spots distribution for a fractal surface with $H = 0.8$, $L = 200$ μm, $q_0 = 2q_L$, $h_{rms} = 1.04$ μm, with $N = 128$ (red spots) and $N = 256$ (green spots). Material properties are $E = 70$ GPa, $\nu = 0.3$ and $\sigma_Y/E^* = 3.25 \times 10^{-2}$. Results are shown for $F/(E^* A_0) \sim 0.0017$.

Results show linearity of the area-load relation, in agreement with existing literature [18]. The values of the slope $k$ of the area-load curves are collected in Fig. 2b. We observe that k takes values much higher than the elastic case (where $k \sim 2$, [3,4,49,50]) and increases with decreasing $\sigma_Y/E^*$, showing that plasticity effects are significant for micrometric rms roughness amplitudes. Non-linearity of the area-load relation is expected for larger values of the contact area [15] and when bulk plastic deformation becomes predominant [51]. However, we are assuming that plastic deformations occur at the asperity level, which is realistic for micro(nano)-metric surface roughness amplitudes [29], and in the investigated range of contact area.

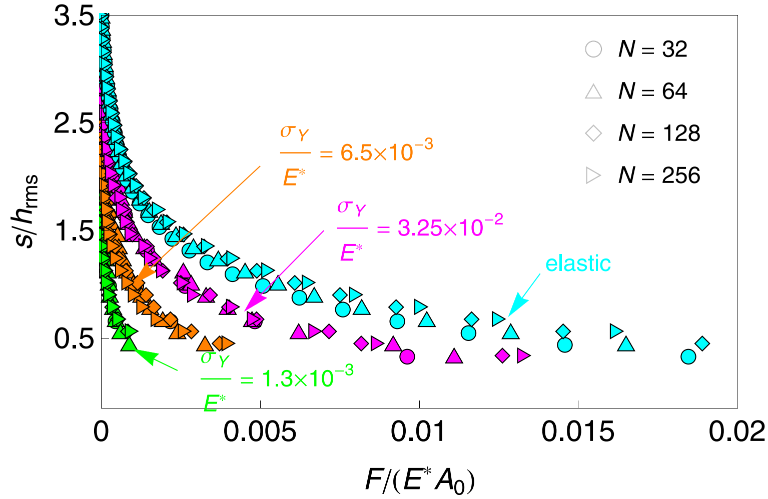


**Fig. 7.** The normalized mean separation $s/h_{rms}$ as a function of the adimensional applied load $F/(E^* A_0)$. Results are shown for fractal surfaces with $H = 0.8$, $N = 32, 64, 128, 256$, $L = 200$ μm, $q_0 = 2q_L$, with $h_{rms} = 1.04$ μm. Material properties are $E = 70$ GPa, $\nu = 0.3$ and $\sigma_Y/E^* = (1.3,\ 6.5,\ 32.5)\times10^{-3}$.

To investigate the contact behavior at nanometric values of $h_{rms}$ we have performed calculations on surfaces with $h_{rms} = 1$, 100 nm, and $H = 0.8$, $N = 128$, $L = 200$ μm, using $2048\times2048$ discretization points. Moreover, a roll-off wave vector $q_0 = 2q_L$ has been fixed to reduce deviations from a Gaussian surface. Finally, we have considered the following yield strength values $\sigma_Y/E^* = (1.3,\ 3.25,\ 32.5)\times10^{-3}$ in the simulations.

Fig. 3a shows the adimensional contact area $A/A_0$ in terms of the normalized load $F/(E^* A_0 h'_{rms})$ for $h_{rms} = 100$ nm. Moving towards higher values of $\sigma_Y/E^*$, namely when plastic effects are less important, ICHA model (markers) predicts a higher contact area than Persson's theory (solid lines). Such a difference can be related to various aspects. First, in the linear elastic case, Persson's theory predicts $A \sim 1.6F/(E^* h'_{rms})$; however, there is consensus in the literature that the elastic asymptotic limit is $A \sim 2F/(E^* h'_{rms})$ [2,4]. In this regard, Persson himself derived a new version of his elastic theory [52], revising the calculation of the elastic energy stored in the contact regions. In the present work, we are considering the elasto-plastic solution of Persson [15,16], where, to the best of the authors knowledge, a similar correction has not been implemented. Furthermore, Persson's theory assumes a constant hardness $H_G = 2.8\ \sigma_Y$, while in ICHA model $H_G$ is a function of the contact penetration.

Fig. 3B gives the same results for $h_{rms} = 1$ nm. Both ICHA model and Persson's theory show all curves collapsing on the elastic solution. These results are in agreement with the findings of Venugopalan et al. [26], where dislocation dynamics has been exploited to simulate the contact between rigid rough profiles and an elasto-plastic half-plane.

In our model plasticity occurs when the asperity penetration reaches the value $\delta_t = 1.9\left(\frac{\pi c \sigma_Y}{2E^*}\right)^2 R$, being $R$ the radius of curvature of the asperity. For a rough surface, the average radius of curvature $\rho$ is related to the rms roughness curvature $h''_{rms}$, being $\rho \approx 1/h''_{rms}$. In our calculations, $h''_{rms}$ is about 1/100 times lower when scaling $h_{rms}$ from 100 nm to 1 nm (as a result, $\rho$ is 100 times higher). Therefore, larger asperity penetrations are required to reach the onset of plasticity when $h_{rms} = 1$ nm, explaining results of Fig. 3b. Moreover, this agrees with the general point of view that smaller $h_{rms}$ usually stands for surfaces with smoother asperities. Therefore, stress concentrations on the peak of asperities reduces when decreasing $h_{rms}$ and, as a result, the plastic deformation on the summits becomes less.

Similar considerations can be deduced from Figs. 4a–b, where the adimensional mean separation $s/h_{rms}$ is given in terms of the load $F/(E^* A_0 h'_{rms})$ for rms roughness of 100 nm and 1 nm, respectively. The mean separation is a key quantity for estimating the contact stiffness, which in turns can be exploited to predict thermal and electrical contact resistance (Refs. [53,54]). Again, we observe that the contact response converges to the elastic solution when higher $\sigma_Y$ and smaller $h_{rms}$ are considered, in agreement with previous theoretical findings [55] ("*...plastic deformations only involves very short-wavelength, ... which will influence the average separation only at very high contact pressures...*"), where the contact mechanics quantities are calculated according to Persson's contact theory and under the assumption that plasticity occurs when the pressure reaches the penetration hardness of the material $\sigma_Y$.

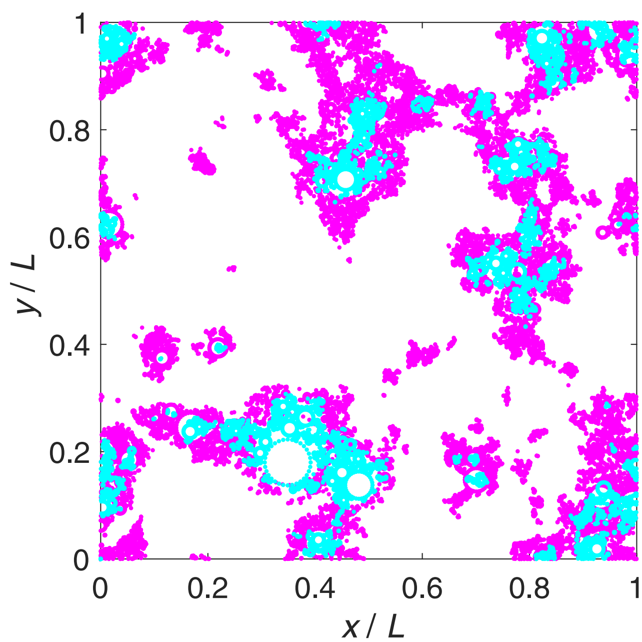


**Fig. 8.** The spots distribution for a fractal surface with $H = 0.8$, $L = 200$ μm, $q_0 = 2q_L$, $h_{rms} = 1.04$ μm with $N = 256$. Material properties are $E = 70$ GPa, $\nu = 0.3$. Results are shown for $F/(E^* A_0) \sim 0.005$, in the elastic case (cyan spots) and for $\sigma_Y/E^* = 32.5\times10^{-3}$ (magenta spots).

The rms gradient $h'_{rms}$ is affected by the high-frequency cut-off $q_1 = Nq_0$ of the roughness spectrum. Increasing $N$ is equivalent to add *fine scale* roughness components to the surface topography. To

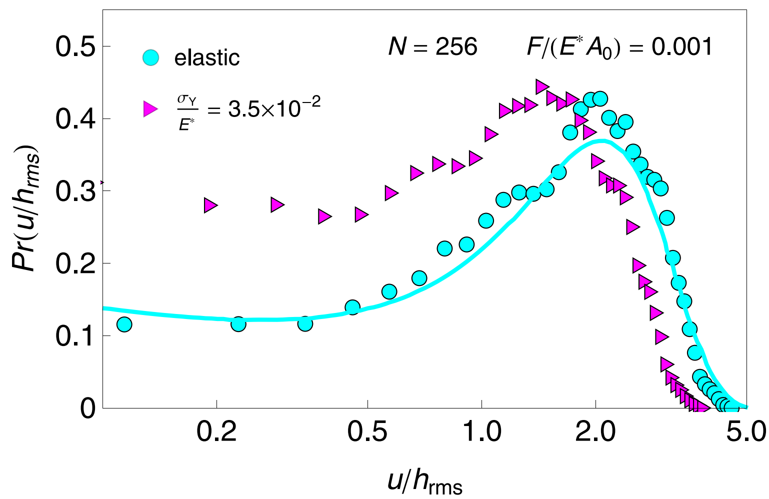


**Fig. 9.** The gap probability distribution $\Pr(u/h_{\rm rms})$ for a fractal surface with $H = 0.8$, $L = 200$ μm, $q_0 = 2q_L$, $h_{\rm rms} = 1.04$ μm, and $N = 256$. Material properties are $E = 70$ GPa, $\nu = 0.3$. Results are shown for $F/(E^* A_0) \sim 0.001$, in the elastic case (cyan) and for $\sigma_Y/E^* = 32.5 \times 10^{-3}$ (magenta). Markers refer to ICHA model, while cyan solid line shows the predictions of Persson elastic theory.

investigate the role of fine scale roughness, in the following we consider fractal surfaces with increasing number of scales $N = 32, 64, 128, 256$. Moreover, we fix $h_{\rm rms} = 1.04$ μm, $q_0 = 2q_L$, $H = 0.8$, $L = 200$ μm and use $2048 \times 2048$ discretization points.

Fig. 5 shows the adimensional contact area $A/A_0$ as a function of the normalized load $F/(E^* A_0)$. As expected, in the elastic case the real contact area reduces for increasing $N$, as a larger load is required to establish the same contact area. In the fractal limit ($N \to \infty$) the contact area tends to vanish (see, for example, Refs. [5,6]). Interestingly, this effect is not observed when plasticity occurs as all curves collapse into a single one. This suggests that plastic deformations destroy fine scale roughness components, whose contribution is no longer fundamental to predict the slope of the area-load curve. In ICHA model, when plasticity occurs, small loads are sufficient to cause coalescence of merging contact spots and to determine larger contact areas. Fig. 6 shows the spatial distribution of contact spots for the same surface realization with $N = 128$ (red spots) and $N = 256$ (green spots). Results are shown for $F/(E^* A_0) \sim 0.0017$ and $\sigma_Y/E^* = 3.25 \times 10^{-2}$. The corresponding contact area is $A/A_0 \sim 0.034$, independently of the number of scales $N$. However, some marginal differences can be observed in the spots distributions as the implementation of coalescence is based on an empirical law.

Fig. 7 shows the adimensional separation $s/h_{\rm rms}$ in terms of the applied load $F/(E^* A_0)$. It is known that $N$ negligibly affects the separation-load curves in the elastic case [3], but our results show that this is especially true when plastic deformations occur.

Fig. 8 shows, at fixed applied load, the modification of the contact regions when plasticity occurs. Specifically, it shows the contact spots distribution for a surface with $N = 256$ under a load $F/(E^* A_0) \sim 0.005$, for the elastic case $\sigma_Y/E^* \to \infty$ (cyan spots) and for $\sigma_Y/E^* = 32.5 \times 10^{-3}$ (magenta spots). The resulting contact areas are, respectively, $A/A_0 \sim 0.04$ and $A/A_0 \sim 0.1$.

We expect that the plasticity-induced enhancement of the contact area also affects local contact quantities. This clearly emerges in Fig. 9, where the gap probability distribution $\Pr(u/h_{\rm rms})$, for $N = 256$ and $F/(E^* A_0) \sim 0.001$, is shown for the elastic case $\sigma_Y/E^* \to \infty$ and for $\sigma_Y/E^* = 32.5 \times 10^{-3}$. The prediction of Persson's theory (cyan solid line) in the elastic limit is also shown, being $\Pr(u/h_{\rm rms})$ computed as proposed in Ref. [4]. The probability $\Pr(u/h_{\rm rms})$ is a critical quantity for estimating percolation [56] and adhesion at the interface [57–59]. The probability of finding smaller gaps increases due to plasticity as an effect of the contact area enhancement, which determines a reduction of the mean separation.

## 4. Conclusions

ICHA model [28] has been extended to the elasto-plastic case by implementing the asperity contact model of Jackson & Green [35]. In agreement with previous studies [55], where the yield stress is assumed independent of the asperity size as in our model, we find that effects of plasticity are negligible for rms roughness amplitude $h_{\rm rms}$ of the order of a few nanometers, as large penetrations should be required for plastic deformations to occur. On the contrary, the contact response is strongly affected by the value of the yield stress $\sigma_Y$ for micrometric $h_{\rm rms}$, even when small loads (large separations) are considered.

In the elastic case, we know the contact area-load relation is affected by $h'_{\rm rms}$ whose value depends on the high-frequency cut-off of the roughness spectrum and is intrinsically related to the instrument sensitivity in roughness measurements. In presence of plasticity, the dependence of the area-load relation on the number of roughness scales is lost as plastic deformations destroy short wavelength roughness. As a result, their contribution is no longer crucial to predict the real contact area, in contrast with what happens in the purely elastic regime.

## CRediT authorship contribution statement

**G. Violano:** Conceived the presented idea, Developed the theory and the computational model (elastoplastic version of the ICHA model), Discussed the results, Contributed to the final manuscript. **L. Afferrante:** Conceived the presented idea, Developed the elastic version of the ICHA model, Contributed to the final manuscript.

## Declaration of competing interest

The authors declare that they have no known competing financial interests or personal relationships that could have appeared to influence the work reported in this paper.

## Data availability

Data will be made available on request.

## References


[1] Persson BN. Theory of rubber friction and contact mechanics. J Chem Phys 2001;115(8):3840–61.
[2] Campañá C, Müser MH. Contact mechanics of real vs. randomly rough surfaces: A green's function molecular dynamics study. Europhys Lett 2007;77(3):38005.
[3] Putignano C, Afferrante L, Carbone G, Demelio G. The influence of the statistical properties of self-affine surfaces in elastic contacts: A numerical investigation. J Mech Phys Solids 2012;60(5):973–82.
[4] Afferrante L, Bottiglione F, Putignano C, Persson BNJ, Carbone G. Elastic contact mechanics of randomly rough surfaces: an assessment of advanced asperity models and Persson's theory. Tribol Lett 2018;66(2):1–13.
[5] Ciavarella M, Demelio G, Barber JR, Jang YH. Linear elastic contact of the Weierstrass profile. Proc R Soc Lond Ser A Math Phys Eng Sci 2000;456(1994):387–405.
[6] Afferrante L, Ciavarella M, Demelio G. Adhesive contact of the weierstrass profile. Proc R Soc A: Math, Phys Eng Sci 2015;471(2182):20150248.
[7] George J, Mannepalli S, Mangalampalli KS. Understanding nanoscale plasticity by quantitative in situ conductive nanoindentation. Adv Energy Mater 2021;23(9):2001494.
[8] Dehm G, Jaya BN, Raghavan R, Kirchlechner C. Overview on micro-and nanomechanical testing: New insights in interface plasticity and fracture at small length scales. Acta Mater 2018;142:248–82.
[9] Vakis AI, Yastrebov VA, Scheibert J, Nicola L, Dini D, Minfray C, et al. Modeling and simulation in tribology across scales: An overview. Tribol Int 2018;125:169–99.
[10] Persson BN, Albohr O, Tartaglino U, Volokitin AI, Tosatti E. On the nature of surface roughness with application to contact mechanics, sealing, rubber friction and adhesion. J Phys: Condens Matter 2004;17(1):R1.
[11] Wang X. (PhD dissertation), 2017.
[12] Chang WR, Etsion I, Bogy DB. An elastic–plastic model for the contact of rough surfaces. 1987.
[13] Zhao Y, Maietta DM, Chang L. An asperity microcontact model incorporating the transition from elastic deformation to fully plastic flow. J Tribol 2000;122(1):86–93.
[14] Jackson RL, Green I. A statistical model of elasto-plastic asperity contact between rough surfaces. Tribol Int 2006;39(9):906–14.
[15] Persson BNJ. Elastoplastic contact between randomly rough surfaces. Phys Rev Lett 2001;87(11):116101.
[16] Xu Y, Li X, Mulvihill DM. Revisiting the persson theory of elastoplastic contact: A simpler closed-form solution and a rigorous proof of boundary conditions. Tribol Lett 2022;70(3):1–7.
[17] Carvalho RP, Carneiro AC, Pires FA, Doca T. An efficient multiscale strategy to predict the evolution of the real contact area between rough surfaces. Tribol Int 2022;165:107255.
[18] Pei L, Hyun S, Molinari JF, Robbins MO. Finite element modeling of elasto-plastic contact between rough surfaces. J Mech Phys Solids 2005;53(11):2385–409.
[19] Zhang F, Liu J, Ding X, Wang R. Experimental and finite element analyses of contact behaviors between non-transparent rough surfaces. J Mech Phys Solids 2019;126:87–100.
[20] Liang XM, Ding Y, Duo Y, Yuan WK, Wang GF. Elastic-perfectly plastic contact of rough surfaces: An incremental equivalent circular model. J Tribol 2021;144(5):051501.
[21] Frérot L, Bonnet M, Molinari JF, Anciaux G. A Fourier-accelerated volume integral method for elastoplastic contact. Comput Methods Appl Mech Engrg 2019;351:951–76.
[22] Zhang W, Lu Z, Chen Y, Zhang Y. Contact analysis between rough surfaces considering the size-affected deformation behaviour of multi-scale asperities. Tribol Int 2022;172:107592.
[23] You S, Tang J, Wen Y. Three-dimensional elastoplastic contact analysis of rough surface considering a micro-scale effect. J Tribol 2022;144(1).
[24] Almqvist A, Sahlin F, Larsson R, Glavatskih S. On the dry elasto-plastic contact of nominally flat surfaces. Tribol Int 2007;40(4):574–9.
[25] Venugopalan SP, Müser MH, Nicola L. Green's function molecular dynamics meets discrete dislocation plasticity. Modelling Simul Mater Sci Eng 2017;25(6):065018.
[26] Venugopalan SP, Irani N, Nicola L. Plastic contact of self-affine surfaces: Persson's theory versus discrete dislocation plasticity. J Mech Phys Solids 2019;132:103676.
[27] Tiwari A, Almqvist A, Persson BNJ. Plastic deformation of rough metallic surfaces. Tribol Lett 2020;68(4):1–12.
[28] Afferrante L, Carbone G, Demelio G. Interacting and coalescing hertzian asperities: a new multiasperity contact model. Wear 2012;278:28–33.
[29] Yusof NFM, Ripin ZM. A technique to measure surface asperities plastic deformation and wear in rolling contact. Wear 2016;368:496–504.
[30] Zhang S, Liu Y, Li X. Effect of plasticity and coalescing for neighboring asperities in contact with a rigid flat. Internat J Modern Phys C 2022;2250120.
[31] Violano G, Afferrante L. Modeling the adhesive contact of rough soft media with an advanced asperity model. Tribol Lett 2019;67(4):1–7.
[32] Violano G, Afferrante L. Contact of rough surfaces: Modeling adhesion in advanced multiasperity models. Proc Inst Mech Eng, Part J: J Eng Tribol 2019;233(10):1585–93.
[33] Li LY, Wu CY, Thornton C. A theoretical model for the contact of elastoplastic bodies. Proc Inst Mech Eng C 2001;216(4):421–31.
[34] Kogut L, Etsion I. Elastic–plastic contact analysis of a sphere and a rigid flat. J Appl Mech 2002;69(5):657–62.
[35] Jackson RL, Green I. A finite element study of elasto-plastic hemispherical contact against a rigid flat. J Tribol 2005;127(2):343–54.
[36] Ghaednia H, Wang X, Saha S, Xu Y, Sharma A, Jackson RL. A review of elastic–plastic contact mechanics. Appl Mech Rev 2017;69(6).
[37] Jackson RL. Discussion of ghaednia, H., Wang, X., Saha, S., Xu, Y., Sharma, A., & Jackson, RL 2017. A review of elastic–plastic contact mechanics. Applied Mechanics Reviews, 69 (6). Appl Mech Rev 2022;74(4):045501.
[38] Wang GF, Liang XM, Yan D. An incremental equivalent circular contact model for rough surfaces. J Tribol 2021;143(8).
[39] Johnson KL. Contact mechanics. Cambridge University Press; 1985.
[40] Besharatloo H, Wheeler JM. Influence of indentation size and spacing on statistical phase analysis via high-speed nanoindentation mapping of metal alloys. J Mater Res 2021;36(11):2198–212.
[41] Xiao Y, Besharatloo H, Gan B, Maeder X, Spolenak R, Wheeler JM. Combinatorial investigation of Al–Cu intermetallics using small-scale mechanical testing. J Alloys Compd 2020;822:153536.
[42] Zhu TT, Bushby AJ, Dunstan DJ. Materials mechanical size effects: A review. Mater Technol 2008;23(4):193–209.
[43] Gorji MB, Furmanski J, Mohr D. From macro-to micro-experiments: Specimen-size independent identification of plasticity and fracture properties. Int J Mech Sci 2021;199:106389.
[44] Song H, Van der Giessen E, Liu X. Strain gradient plasticity analysis of elasto-plastic contact between rough surfaces. J Mech Phys Solids 2016;96:18–28.
[45] Song H, Vakis AI, Liu X, Van der Giessen E. Statistical model of rough surface contact accounting for size-dependent plasticity and asperity interaction. J Mech Phys Solids 2017;106:1–14.
[46] Hutchinson JW. Plasticity at the micron scale. Int J Solids Struct 2000;37(1–2):225–38.
[47] Bushby AJ, Dunstan DJ. Plasticity size effects in nanoindentation. J Mater Res 2004;19(1):137–42.
[48] Zhao Y, Chang L. A model of asperity interactions in elastic–plastic contact of rough surfaces. J Tribol 2001;123(4):857–64.
[49] Putignano C, Afferrante L, Carbone G, Demelio G. A new efficient numerical method for contact mechanics of rough surfaces. Int J Solids Struct 2012;49:338–43.
[50] Muser MH, Dapp WB, Bugnicourt R, Sainsot P, Lesaffre N, Lubrecht TA, et al. Meeting the contact-mechanics challenge. Tribol Lett 2017;65(118).
[51] Stupkiewicz S, Mróz Z. Phenomenological model of real contact area evolution with account for bulk plastic deformation in metal forming. Int J Plast 2003;19(3):323–44.
[52] Persson BNJ. On the elastic energy and stress correlation in the contact between elastic solids with randomly rough surfaces. J Phys: Condens Matter 2008;20(31):312001.
[53] Barber J. Bounds on the electrical resistance between contacting elastic rough bodies. Proc R Soc Lond Ser A Math Phys Eng Sci 2003;459(2029):53–66.
[54] Afferrante L, Carbone G, Putignano C, Violano G, Demelio G. Thermoelastic effects in the contact mechanics of 1D+1D rough profiles. Int J Solids Struct 2022;253:111635.
[55] Persson BNJ. Leakage of metallic seals: role of plastic deformations. Tribol Lett 2016;63(3):1–6.
[56] Putignano C, Afferrante L, Carbone G, Demelio GP. A multiscale analysis of elastic contacts and percolation threshold for numerically generated and real rough surfaces. Tribol Int 2013;64:148–54.
[57] Violano G, Demelio GP, Afferrante L. On the DMT adhesion theory: from the first studies to the modern applications in rough contacts. Procedia Struct Integr 2018;12:58–70.
[58] Violano G, Afferrante L. On DMT methods to calculate adhesion in rough contacts. Tribol Int 2019;130:36–42.
[59] Persson BN, Scaraggi M. Theory of adhesion: Role of surface roughness. J Chem Phys 2014;141(12):124701.